RAPID COMMUNICA

PHYSICAL REVIEW B, VOLUME 64, 241102(R)

Intrinsic birefringence in calcium fluoride and barium fluoride

John H. Burnett, Zachary H. Levine, and Eric L. Shirley
National Institute of Standards and Technology, Gaithersburg, Maryland 20899
(Received 14 May 2001; revised manuscript received 26 September 2001; published 29 November 2001)

We report measurements of the intrinsic birefringence in CaF_2 and BaF_2 for wavelengths in the range 365 nm to 156 nm, and *ab initio* optical response calculations in these materials and Si, Ge, GaAs, and GaP. Calculations typically agree within 40%. For ⟨110⟩ propagation, where the effect is largest, our measurements for $CaF_2[BaF_2]$ give $n_{\langle\bar{1}10\rangle}-n_{\langle001\rangle}=(-11.8\pm0.4)\times10^{-7}[(+34\pm3)\times10^{-7}]$ for $\lambda=156.10$ nm. The magnitudes of these values have serious consequences for the use of crystalline optics in precision optical systems in the ultraviolet, including 193 nm and 157 nm optical lithography.

DOI: 10.1103/PhysRevB.64.241102

PACS number(s): 78.20.Fm, 78.20.Bh

Optics for the visible and near ultraviolet are generally made of glassy materials, in part because of their inherent isotropic optical properties. However, their use in the deep and vacuum ultraviolet (VUV) is limited by their high absorption at these wavelengths. For precision optics in the VUV, cubic crystalline materials with shorter-wavelength transmission cutoffs are used, especially CaF_2. The cubic symmetry is generally presumed to ensure isotropy of the optical properties such as absorption and index of refraction. However, as pointed out by Lorentz, even prior to the formulation of the macroscopic Maxwell equations, the isotropy of cubic crystals should be broken at short wavelengths because of a symmetry breaking from the finite value of the wave vector $\mathbf{q}$ of the light, resulting in an intrinsic birefringence.[1,2]

Measurements of this effect, also known as spatial-dispersion-induced birefringence, have been made on a number of semiconductors and insulators, including Si,[3] Ge,[4] GaAs,[5–7] GaP,[6,8] ZnTe, ZnS,[8] ZnSe,[8,9] CuCl,[10] CuBr, CuI,[11] KI,[12–13] NaCl, KCl, RbCl, NaBr, KBr, RbBr, CsBr, NaI, RbI, and CsI.[13] In this paper we report measurements of the intrinsic birefringence in the range 365 nm to 156 nm, of CaF_2, the most widely used crystalline material for precision optics in the VUV, and BaF_2, an alternate VUV material. First-principles calculations of the intrinsic birefringence are also presented here. (Earlier, effective-mass-type calculations also analyzed the birefringence, but were necessarily more empirical.) Our calculations quantitatively confirm our measurements for CaF_2 and BaF_2, and other measurements for Si, Ge, GaAs, and GaP. The magnitudes of the results for the fluorides have serious implications for the performance of precision optical systems in the VUV, including imaging systems, spectrometers, and interferometers, that use crystalline optical components, such as lenses, beamsplitters, and windows. For example, the value for CaF_2 at 156.10 nm, $n_{\langle\bar{1}10\rangle}-n_{\langle001\rangle}=(-11.8\pm0.4)\times10^{-7}$ for $\hat{\mathbf{q}}\|\langle110\rangle$, is greater than ten times the target specification for material birefringence in 157 nm lithography systems.[14] (In this paper, we quote total standard uncertainties.)

Our measurement method is based on determining the amount of phase compensation needed to null out light transmitted through an oriented sample between crossed polarizers.[3] Measuring the effect as a function of wavelength in the VUV required operation in an oxygen-free, nitrogen-purge environment with VUV polarizers and a phase compensator, and using as illumination sources a series of VUV atomic spectral lines. These were obtained from carbon I emission from CO_2 introduced in a custom argon mini-arc lamp, filtered though a monochromator.[15] The longer-wavelength UV measurements were made using an electrodeless Hg lamp. The spectral line emission was chopped, collimated by a paraboloidal mirror, and linearly polarized by a MgF_2 Rochon polarizer. The polarized light passed through the sample on a rotation stage and a MgF_2 Soleil-Babinet compensator oriented 45° to the polarizer, and impinged on a crossed MgF_2 Rochon polarizer. Light that was transmitted through the crossed polarizer, as a result of birefringence of the sample or compensator, was detected by a CsI or CsSb photomultiplier tube, using a lock-in amplifier. By varying the sample mounting orientation, we demonstrated that effects of residual stress birefringence from the sample mounting were negligible.

We studied four single-crystal samples of CaF_2 from three different suppliers, which were of the form of rectangular parallelepipeds or cubes with propagation-direction thicknesses, 12, 20, 25, and 30 mm. Three samples each had polished faces normal to [110], [$\bar{1}$10], and [001] directions (type I), and one sample had polished faces normal to [111], [$\bar{1}$10], and [11$\bar{2}$] directions (type II). Back-reflection Laue measurements confirmed these orientations to within 2°. Low values of intrinsic stress in one of the samples were confirmed by stress-birefringence measurements at 633 nm, showing rms values of <0.20 nm/cm. We also studied two single-crystal samples of BaF_2 of each of the two sample types.

For every orientation of each sample, two sets of measurements were made. First, the compensator was adjusted for zero compensation, and the transmitted intensity through the crossed polarizer was measured as a function of the angle between a crystal axis and the plane of polarization. The birefringence Δn was determined by fitting these results to the equation: $I/I_0=\sin^2(\pi d\Delta n/\lambda)\sin^2(2\theta)$, where I/I_0 is the ratio of the transmitted light at a given angle to the maximum at π relative phase and d is the thickness of the sample in the transmission direction.[12] Figure 1(a) shows results for a type I sample using 156.10 nm radiation with $\hat{\mathbf{q}}\|[110]$. The horizontal axis represents the angle between the [001] sample direction and the plane of polarization.

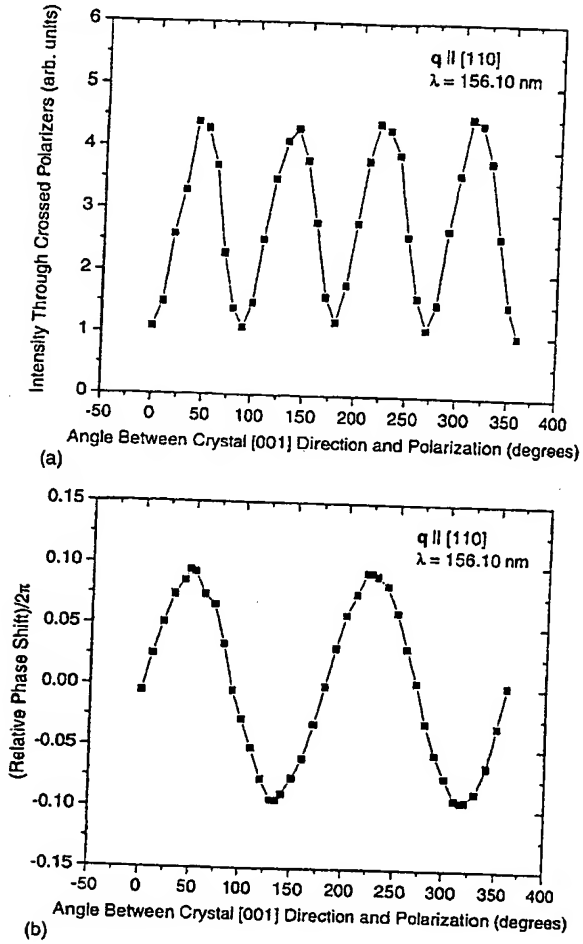

FIG. 1. (a) Intensity through crossed polarizers vs angle between crystal [001] direction and the plane of polarization for $\hat{q}\|[110]$ and $\lambda = 156.10$ nm. Sample thickness is 12.0 mm. (b) Relative phase shift divided by 2π for two orthogonal directions 45° from the plane of polarization vs angle between crystal [001] direction and the plane of polarization, for $\hat{q}\|[110]$ and $\lambda = 156.10$ nm. Sample and geometry are the same as for 1(a).

In a second series of measurements, the phase compensator was adjusted for each sample angle to zero the transmitted intensity by compensating the sample birefringence. This determined the angular dependence of the relative phase shift through the sample between the two orthogonal polarizations. The birefringence was derived from the maximum relative phase shift observed and the sample thickness. Figure 1(b) shows the results for the same sample, wavelength, and sample orientations as in Fig. 1(a). The extrema in the relative phase shift occur for the orientation of the sample [001] direction 45°, 135°, 225°, and 315° from the polarization direction, corresponding to the maximum transmission intensities in Fig. 1(a), as expected. The orientation of the MgF_2 compensator gave the sign of the birefringence. The birefringence determined by the two methods above were consistent within 20% for all samples, though the compensator method was inherently more accurate, and these are the values presented. The birefringence was measured in this fashion for two equivalent $\langle 110 \rangle$ propagation directions in each of the three similar CaF_2 samples, and for each sample the values were within 5% of the average. Sample thicknesses varied by over a factor of 2, and the results were the same within the estimated uncertainties, supporting our interpretation of the measured birefringence as a bulk property. A similar set of measurements was made for $\hat{q}\|[001]$ for the type I samples and for $\hat{q}\|[111]$ for the type II samples, and the observed birefringence was zero within the uncertainties for both directions. We also made this complete set of measurements for the BaF_2 type I and type II samples.

The value of the birefringence $\Delta n = n_{\langle \bar{1}10 \rangle} - n_{\langle 001 \rangle}$ was determined for CaF_2 for six wavelengths from 365.06 to 156.10 nm, and the results, averaged over the samples, are presented in Table I along with calculations discussed later. The table shows that measured CaF_2 data and calculations both have a sign change, between 193.09 and 365.06 nm. Measurements and calculations for BaF_2 are also presented in Table I, which shows that the values for BaF_2 are of opposite sign to those for CaF_2 at the shorter wavelengths. These measurements are plotted in Figs. 2(a) and 2(b) along with the calculations [the individual measurements on the different samples are presented in Fig. 2(b)]. These results show that the birefringence is small ($<10^{-7}$ for CaF_2) for $\lambda = 365$ nm, and increases rapidly for shorter wavelengths [consistent with a $1/\lambda^2(q^2)$ dependence, cf. Eq. (1)], explaining why the effect has not

TABLE I. Measurements and calculations of birefringence of CaF_2 and BaF_2 in the UV. Values at each wavelength averaged over measurements for samples from N different suppliers.

	CaF_2 $10^7 \times (n_{\langle \bar{1}10 \rangle} - n_{\langle 001 \rangle})$			BaF_2 $10^7 \times (n_{\langle \bar{1}10 \rangle} - n_{\langle 001 \rangle})$		
Wavelength (nm)	N	measured	(calculated)	N	measured	(calculated)
365.06 (Hg I)	2	0.19±0.04	(0.66)	1	4.0±0.6	(5.3)
253.65 (Hg I)	2	−0.55±0.07	(0.84)	1	9.5±1.1	(12.7)
193.09 (C I)	3	−3.4±0.2	(−1.4)	1	19±2	(26.9)
175.19 (C I)	1	−5.7±0.3	(−5.2)	1	25±2	(36.4)
165.72 (C I)	1	−8.3±0.4	(−9.9)	1	29±2	(43.6)
156.10 (C I)	3	−11.8±0.4[a]	(−19.7)	1	34±3	(52.7)

[a]Interpolated value for CaF_2 at the excimer laser wavelength 157.63 nm is $\Delta n = (-11.2 \pm 0.4) \times 10^{-7}$.

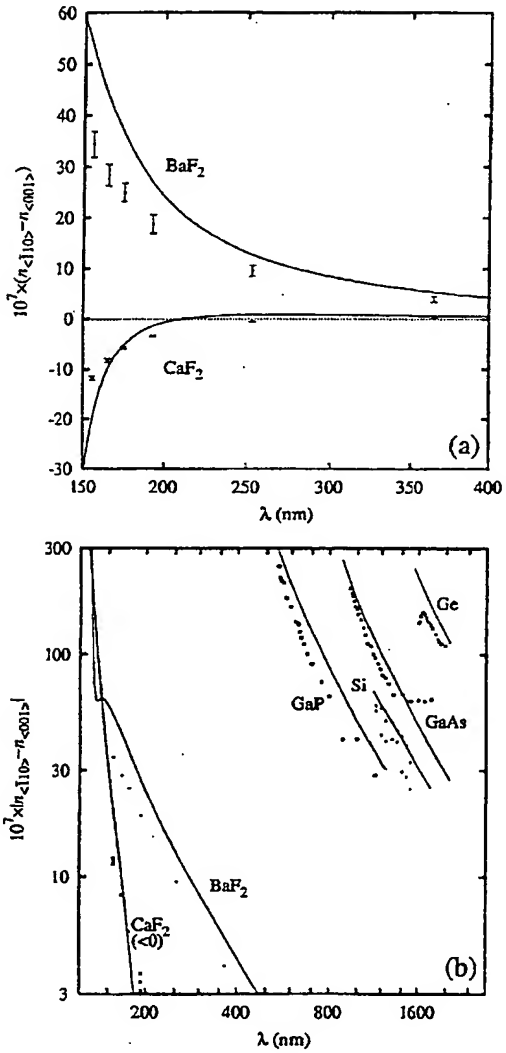

FIG. 2. (a) Measured (symbols) and calculated (curves) birefringence $\Delta n=(n_{\langle\bar{1}10\rangle}-n_{\langle 001\rangle})$ for CaF_2 and BaF_2 for $\hat{q}\|[110]$ vs wavelength. (b) Magnitude (log plot) of measured and calculated birefringence vs wavelength for semiconductors, along with CaF_2 and BaF_2. (Measured results for Si, Ge, GaAs, and GaP are taken from Refs. 3, 4, 5, and 8, respectively.) All values are positive, except for CaF_2, whose values are negative in experiment and theory at short wavelengths, with a zero crossing near 200 nm (theory) or 300 nm (measurement).

been an issue for precision crystalline optics at longer wavelengths. This high dispersion also rules out spurious stress birefringence, because of the much lower dispersion of the piezo-optical coefficients for CaF_2 and BaF_2.[16] Note that the values of the birefringence at 193.09 and at 156.10 nm are large compared to the low-birefringence requirements of a number of precision UV high-numerical-aperture optics applications, in particular 193-nm lithography and 157-nm lithography technologies now under development. [The 157-nm lithography target specification is $\Delta n=1\times10^{-7}$ for 157 nm (Ref. 14).]

Symmetry analysis elucidates many aspects of the birefringence, including its dependence on propagation direction. For a cubic crystal, the dielectric tensor may be expanded in wave vector as[17]

$$\varepsilon_{ij}(\mathbf{q},\omega)=\varepsilon(\omega)\delta_{ij}+\Sigma_{kl}\alpha_{ijkl}(\omega)q_kq_l+\ldots, \qquad (1)$$

where δ_{ij} is Kronecker's δ. The product q_kq_l and symmetry of ε_{ij} show that α_{ijkl} is symmetric under interchanges $i\leftrightarrow j$ and $k\leftrightarrow l$.[17] Further, cubic symmetry reduces the number of independent components to the three familiar ones from elasticity theory.[18] An isotropic system permits two independent tensor components.[18] One component represents an inconsequential change in ε proportional to q^2; the other represents an isotropic longitudinal-transverse splitting. In practice, $\Sigma_{kl}\alpha_{ijkl}q_kq_l$ is a very small correction to ε, so neglecting terms of order q^4, the propagating waves are purely transverse. The third component that exists in a cubic system (but does not exist in an isotropic system) determines all observable anisotropies. Only this component need be considered. The related tensor elements, α_{1111}, α_{1122}, and α_{2323}, appear in the ratio $2:-1:-1$, and this determines the angle dependence. For $\mathbf{q}=(1,1,0)/2^{1/2}$, the scaled eigenvalues of the contracted tensor $\Sigma_{kl}\alpha_{ijkl}q_kq_l$ are 3/2 and -1 for the transverse $[\bar{1}10]$ and [001] directions, respectively. Measuring the associated birefringence for one propagation direction determines the magnitude of the anisotropic response of the crystal for all propagation directions. Interestingly, a cubic crystal has seven nonbirefringent axes, four in the $\langle111\rangle$ directions and three in the $\langle100\rangle$ directions, with birefringence maxima in the twelve $\langle110\rangle$ directions.

In practice, precision CaF_2 UV lenses are usually made with $\langle111\rangle$ or $\langle100\rangle$ as the axis of propagation. For a circular lens with a given numerical aperture (NA), only the variation in the index for propagation within the included angles will matter. Because there is no birefringence for propagation exactly along $\langle111\rangle$ (or $\langle100\rangle$) and small near these directions, the full effect of the birefringence can be avoided for small NA, but not for the high NA values used in photolithography. The maximum effect is realized for propagation directions within the material of angles $\cos^{-1}[(2/3)^{1/2}]\approx35.26°$ (or 45°). In Fig. 3, the practical effect of the measured birefringence is shown. Azimuthal averages around the [111] and [100] directions are given. The polarization splitting has been measured in this work. However, this splitting also determines the directional dependence of the polarization-averaged dielectric constant, which is also shown and is significant for lens design. Note that the birefringence has a weaker angular dependence near the [100] direction compared to near the [111] direction, because of an extremum in the [100] direction, suggesting an advantage for [100] oriented lenses.

We have also, for the first time, estimated the anisotropy by rigorous first-principles calculations of the dielectric tensor as a function of $\hat{\mathbf{q}}$ and ω. The dielectric tensor was computed using the method of Benedict *et al.*,[19] extended to finite $\mathbf{q}$ according to Soininen and Shirley.[20] These calculations included both local-field and excitonic effects, and took only the crystal structure and static dielectric func-

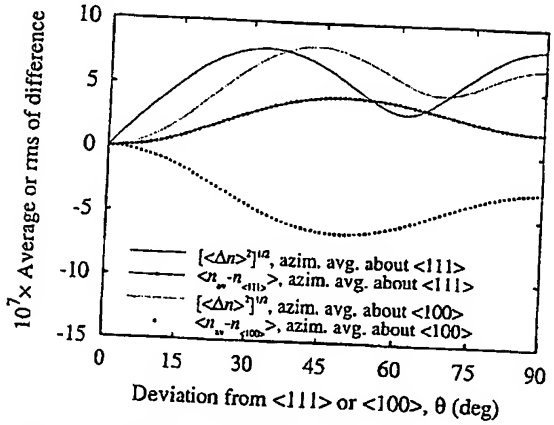

FIG. 3. Index anisotropy, scaled according to $\Delta n = 11.2\times10^{-7}$ for $\hat{q}\|[110]$. Results are shown for quantities azimuthally averaged about a ⟨111⟩ or ⟨100⟩ axis at a given angle of deviation from that axis, θ, as follows: root-mean-squared (rms) index difference (birefringence), and difference between the polarization-averaged index, n_{av}, and the index for propagation along that nonbirefringent axis ($n_{\langle111\rangle}$ or $n_{\langle100\rangle}$).

tion from experiment. Results depended on several numerical convergence parameters, and convergence and consistency tests suggest a 15% relative uncertainty of the birefringence (unless it is accidentally very small). To achieve this precision, several spurious, previously irrelevant symmetry-breaking effects in $\varepsilon(\sim10^{-3})$ were reduced by $\sim10^4$ through program refinements. The present results reflect sampling of all valence bands and 12 conduction bands in the semiconductors, with 1000 Brillouin zone (BZ) points in Ge and GaAs, and 1728 BZ points in Si and GaP. The CaF_2 results reflect sampling of 12 valence and 66 conduction bands and 512 BZ sampling points. BaF_2 results included 24 conduction bands. The results for the fluorides are shown in Fig. 2, with the measurements. Note (cf. Table I) that the sign of Δn is opposite between CaF_2 and the other materials, in experiment and theory for short wavelengths, and there is a zero crossing near 200 nm. The results for the semiconductors are also shown in Fig. 2(b). The typical agreement of these calculations with the measurements for all materials is within 40%, except for CaF_2 near the zero crossing. The agreement in sign, wavelength dependence, and magnitude with the measurements for CaF_2 and BaF_2 further confirms our attribution of the measured effect to spatial-dispersion-induced birefringence. Further, these results demonstrate that the Bethe-Salpeter equation may be applied to a rather subtle phenomenon—the spatial dispersion of the birefringence in cubic materials—which has not been the result of any previous *ab initio* calculation.

The magnitudes of the intrinsic birefringences in cubic crystalline optics determined by measurement and calculation are large enough to have serious consequences for precision UV optical technologies under consideration and development. However, the symmetry of the effect may provide a solution to the difficulties. Combining [111]-oriented ([100]-orientated) lenses with their transverse crystal axes rotated relatively by 60° (45°) provides partial compensation of the birefringence. The opposite sign of the effect for CaF_2 and BaF_2 suggests combining optical components of both materials; moreover, an appropriate mixed solid solution $Ca_{1-x}Ba_xF_2$ could eliminate the effect at a given wavelength.[21]

[1] H. A. Lorentz, *Collected Papers II* (Martinus Nijohff, The Hague, 1936), pp. 1–119, esp. p. 79; Verh. K. Akad. Wet. Amsterdam, Afd. Natuurkd. **18** (1878).

[2] H. A. Lorentz, *Collected Papers III* (Martinus Nijohff, The Hague, 1936), pp. 314–320; Proc. R. Acad. Sci. Amsterdam **24**, 333 (1921).

[3] J. Pastrnak and K. Vedam, Phys. Rev. B **3**, 2567 (1971).

[4] P. Y. Yu and M. Cardona, in *Computational Solid State Physics*, edited by F. Herman *et al.* (Plenum, New York, 1972), p. 7.

[5] P. Y. Yu and M. Cardona, Solid State Commun. **9**, 1421 (1971).

[6] Yu. N. Berozashvili, S. Z. Machavariani, A. G. Natsvlishvili, E. G. Tsitsishvili, and V. Sh. Édilashvili, Sov. Phys. Semicond. **15**, 334 (1981).

[7] P. Etchegoin, A. Fainstein, P. Santos, L. C. Lew Yan Voon, and M. Cardona, Solid State Commun. **92**, 505 (1994).

[8] M. Bettini and M. Cardona, in *Proceedings of the 11th International Conference on the Physics of Semiconductors* (Polish Sci. Pub., Warsaw, 1972), p. 1072.

[9] A. Friberg and I. Holwech, Appl. Phys. **11**, 383 (1976).

[10] E. G. Tsitsishvili, O. V. Gogolin, J. L. Deiss, and V. N. Bagdavadze, Solid State Commun. **56**, 717 (1985).

[11] J. L. Deiss, A. Daunois, A. Chouiyakh, and O. Gogolin, Solid State Commun. **53**, 79 (1985).

[12] F. Meseguer, M. Cardona, and A. Cintas, Solid State Commun. **50**, 371 (1984).

[13] C. Zaldo, C. López, and F. Meseguer, Phys. Rev. B **33**, 4283 (1986).

[14] A. K. Bates, in *Proceedings of the First International Symposium on 157 nm Lithography*, edited by R. Harbison (International SEMATECH, Austin, 2000), p. 377.

[15] J. M. Bridges and W. R. Ott, Appl. Opt. **16**, 367 (1977).

[16] J. H. Burnett, in *Proceedings of 157 nm Technical Data Review*, edited by R. Harbison (International SEMATECH, Austin, 2000).

[17] V. M. Agranovich and V. L. Ginzburg, *Crystal Optics with Spatial Dispersion and Excitons*, 2nd ed. (Springer-Verlag New York, 1984), pp. 129–135.

[18] H. J. Juretschke, *Crystal Physics* (Benjamin, London, 1974), Sections 4.2 and 11.2.

[19] L. X. Benedict and E. L. Shirley, Phys. Rev. B **59**, 5441 (1999), and references therein.

[20] J. A. Soininen and E. L. Shirley, Phys. Rev. B **61**, 16 423 (2000).

[21] http://physics.nist.gov/DUVBirefring